Available online at www.sciencedirect.com
ScienceDirect
International Journal of Multiphase Flow 34 (2008) 636–646
International Journal of Multiphase Flow
www.elsevier.com/locate/ijmulflow

Wave behavior in horizontal annular air–water flow

D. Schubring, T.A. Shedd *

Multiphase Flow Visualization and Analysis Laboratory, University of Wisconsin-Madison, 1500 Engineering Drive, Madison, WI 53706-1609, USA

Received 23 October 2007

Abstract

In this study, non-intrusive pressure drop, liquid base film thickness distribution, and wave behavior measurements have been obtained for 206 horizontal annular two-phase (air–water) flow conditions in 8.8, 15.1, and 26.3 mm ID tubes. Reliable wave velocity measurements are available for 185 of these flow conditions, while 131 flow conditions allow for reliable wave frequency measurements. The wave velocity is found to be predicted to within 9% by gas friction velocity and 6% by an optimized correlation of similar structure. Wave frequency can also be predicted with a simple correlation to within 5% for the 8.8 and 15.1 mm tubes, but a separate relation is required to explain 26.3 mm frequency data. The differences in wave behavior between the annular and wavy-annular/wavy regimes are also discussed.

Keywords: Air–water; Disturbance waves; Horizontal flow; Annular flow; Correlations

1. Introduction

Annular flow in both horizontal and vertical configurations includes two types of wave structures. The first are small ripples on the base film that move at low velocities and do not appear to carry mass. The second structure, disturbance waves, carry mass along the tube. These waves show a larger film thickness than the film between them and travel at a higher velocity. Studies of annular flow have considered these waves as both a component of the film, as in film roughness interfacial shear modeling, and as separate structures, as in the excess liquid hypothesis (see Schadel (1988) among others). This excess liquid hypothesis vis-à-vis wave behavior was explored by Azzopardi and Whalley (1980) who used artificial waves to investigate the volume of liquid entrained in the gas core and contained in waves.

Characterization of the effects of disturbance waves in annular two-phase flow requires knowledge of wave frequencies, velocities, and spacings. Measurement or correlation of two of these parameters allows the third to be calculated. Some correlations and models have been developed; however, the analysis of disturbance waves has not led to the volume of literature seen for pressure drop and interfacial shear modeling.

Experiments in vertical upflow have led to recognition of some general trends, as discussed by Azzopardi (1986). These include the increase of wave velocity and frequency with both gas and liquid flow rates (after Nedderman and Shearer, 1963; Hall Taylor et al. (1963)). Martin (1983) observed no strong dependence of wave velocity on tube diameter for the same gas velocity and a decrease of wave frequency with increasing diameter. For the case of vertical downflow, Thwaites et al. (1976) observed asymptotic behavior with increasing liquid flow at constant gas flow; however, their gas flow rates are lower than those in the present study.

Some researchers (e.g., Mori et al., 1996) have suggested the presence of two types of large wave structures in certain vertical flow conditions. These structures are termed disturbance waves and huge waves, with the latter traveling at

* Corresponding author. Tel.: +1 608 265 2930; fax: +1 608 262 8464.
E-mail address: shedd@engr.wisc.edu (T.A. Shedd).

0301-9322/$ - see front matter © 2008 Elsevier Ltd. All rights reserved.
doi:10.1016/j.ijmultiphaseflow.2008.01.004

greater velocity and consisting of a greater mass of fluid than the former. These huge waves were found near the annular-churn boundary, i.e., at higher liquid superficial velocities and/or lower gas superficial velocities than those seen in the present study. In an investigation of both types of wave structures, Mori et al. (1999) found that wave frequency is inversely related to kinematic viscosity.

Swanson (1966) observed similarity between gas friction velocity and wave velocity, while Pearce (1979) developed a correlation for wave velocities in terms of gas velocity, film surface velocity, and the density ratio between phases. Hall Taylor and Nedderman (1968) as well as Azzopardi (1986) have attempted to use wave coalescence to explain wave frequency and spacing. Their models include observations about the distribution of wave velocities. Correlations developed by Shearer are also included in the paper by Hall Taylor and Nedderman (1968), which applied them to air–water and steam-water data. While Shearer's wave velocity correlation was found to be applicable to the Hall Taylor and Nedderman data, it is for gas flow rates below those in the present study.

More recently, Hawkes et al. (2000) used a similar wave data acquisition method as the present study to consider wave frequency and velocity in vertical geometry. Their study focused on systems with higher liquid flow rates than those in the present work. Two structures are identified in their work: disturbance waves and wisps. Hawkes et al. determined disturbance wave velocities ranged from 10 to 20 m s^{-1}, with frequencies of 15–20 s^{-1}. The wisps identified traveled at a higher velocity, but a lower frequency.

Understanding of wave behavior in horizontal annular flow is still quite limited. Early data were taken in rectangular channel geometry by Zanelli and Hanratty (1971); however, their liquid flow rates were well below those in the present study. The work of Jayanti et al. (1990) primarily focused on explaining film thickness distribution in horizontal geometry; however, they performed analysis of waves as a means to this end. One significant finding was that at sufficiently high gas velocities, such as those in the present study, disturbance waves indeed move at a single velocity around the periphery of the tube. Also working towards understanding film thickness, Paras and Karabelas (1991) provide a small number of wave frequency and velocity data in a 50.8 mm tube. Ottens et al. (1999) developed a model for lower flow rates than those seen in the present study.

The present work aims to compare these correlations and observations to a large bank of data from the fully annular regime in horizontal flow. Empirical correlations for wave velocity and wave frequency are presented. It is hoped that the comparison and development of correlations for disturbance waves will be useful in exploration of the fundamental physics at work for these waves, as well as their interrelationship with other two-phase flow parameters. In particular, the relationship between disturbance waves and shear is explored. Further, some correlations are also applied to wavy-annular flow, a regime not present in vertical geometry.

2. Experimental setup

2.1. Flow loop

The two-phase flow loop used for these experiments is shown in Fig. 1. Laboratory compressed air was delivered to the test section inlet via a bank of variable-area volumetric flow meters. The uncertainties, based on manufacturer's stated values and including density correction, were 8.4 L min^{-1} below 250 L min^{-1} flow, 14 L min^{-1} between 300 and 700 L min^{-1} flow, and 68 L min^{-1} above 700 LPM L min^{-1} flow. A pressure gauge near the flow meters allowed for the correction of flow meter readings to compensate for variations in air density and for the calculation of the mass flow rate entering the test section. Water entered the flow loop through a series of small (1.5 or 3 mm) holes drilled in the test section wall about 150 mm from the air entrance.

The two-phase air–water mixture passed through a flow development length before any measurements were obtained. This length was 400 diameters for the 8.8 mm ID tube, 330 diameters for the 15.1 mm ID tube, and 210 diameters for the 26.3 mm ID tube. The air and water were separated in a gravity-assisted centrifugal separator, after which the water entered a holding reservoir. A variable-speed peristaltic pump was used to draw water from the reservoir through a 40 μm filter. Because of

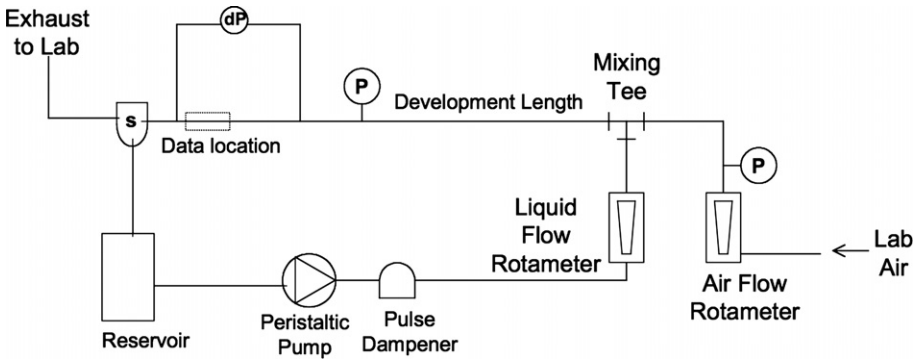

Fig. 1. Diagram of flow loop.

the pulsating nature of peristaltic pumps, a pulse dampening closed reservoir was placed after the pump. The liquid flow was measured using a bank of variable-area rotameters with manufacturer's specified accuracies of 45 $cm^3\,min^{-1}$ for less than 1500 $cm^3\,min^{-1}$ flow, 90 $cm^3\,min^{-1}$ for 1500–3000 $cm^3\,min^{-1}$ flow, and 5% of reading for above 3000 $cm^3\,min^{-1}$ flow. The test sections were constructed of clear PVC (Excelon R4000) for complete visualization of the flow from liquid entrance to exit.

2.2. Pressure measurement

A bourdon-tube gauge was placed near the test section so that a good estimate of local air density could be obtained. In the 15.1 and 26.3 mm ID tubes, this gauge was placed at the beginning of the test section, while it was placed 0.5 m upstream for the 8.8 mm ID tube. The 8.8 mm ID case is shown in Fig. 1. The 0.25 lb in^{-2} reading uncertainty produces an uncertainty on absolute pressure, gas density, gas superficial velocity, and gas kinetic energy of less than 3%.

Using the two static pressure measurements, dry air mass was conserved in calculations. The air entering the test section was assumed to be dry at a temperature of 20 °C. Within the test section, a relative humidity of 100% was assumed at a temperature of 11 °C.

2.3. Data range

For each diameter, an array of meter readings were selected to provide a large bank of data. The 206 fully annular data points are a subset of these data. Superficial gas and liquid velocities were calculated according to Eqs. (1) and (2), with gas kinetic energy calculated according to Eq. (3). In these equations, G is the mass flux, x is the flow quality, $\dot{m}$ is a mass flow rate, KE_{sg} is the gas kinetic energy density (or dynamic pressure), ρ is a density, and A refers to total flow area:

$$U_{sg} = \frac{Gx}{\rho_g} \tag{1}$$

$$U_{sl} = \frac{G(1-x)}{\rho_l} \tag{2}$$

$$KE_{sg} = \frac{U_{sg}^2 \rho_g}{2} \tag{3}$$

$$x = \frac{\dot{m}_g}{\dot{m}_g + \dot{m}_l} \tag{4}$$

$$G = \frac{\dot{m}_g + \dot{m}_l}{A} \tag{5}$$

Superficial gas velocities of between 28 and 86 m s^{-1} were considered, with superficial liquid velocities between 0.045 and 0.30 m s^{-1}. Superficial gas kinetic energy densities ranged from 600 to 5400 J m^{-3} as a result of the variable superficial velocities and gas densities through the test section. The cut-off of 600 J m^{-3} was selected to correspond with changes in trends of pressure drop, film thickness distribution, and wave behavior that may be indicative of a transition from the fully annular behavior studied presently and a separate wavy-annular regime.

Reliable wave data were not available for all points studied. At low liquid flow rates, wave frequency data were not available. At the lowest liquid flow rates, wave velocity data were also not reliable. In total, 21 fully annular flow conditions were discarded, leaving 185 wave velocity measurements. The data included for wave velocity measurement can be seen in Schubring and Shedd (submitted for publication) as arrays of G, x, and P.

It was found that frequency data were more challenging to acquire, particularly for low liquid flows and the highest gas flows. Data that were unreliable, as measured by repeatability of measurement and by the sample standard behavior, are excluded, leaving 131 flow conditions above 0.07 m s^{-1} liquid superficial velocity. The 8.8 mm ID flow conditions of 320 $cm^3\,min^{-1}$ water flow and 130–150 L min^{-1} air flow were also discarded for non-reliable frequency data, as were the 15.1 mm ID conditions of 2500–2900 $cm^3\,min^{-1}$ water flow and 700 L min^{-1} air flow. Finally, 26.3 mm ID flow conditions of 2000 L min^{-1} and above air also failed to produce reliable frequency data and were not used in that analysis.

The correlations used require calculation of several dimensionless parameters, most commonly Reynolds numbers. The most common Reynolds number used in the correlations is defined by

$$Re_G = \frac{GD}{\mu_l} \tag{6}$$

with μ_l as the liquid viscosity.

2.4. Pressure drop measurement

The differential pressure measurement was performed over 1 m for the 15.1 and 26.3 mm ID tubes and over 0.5 m for the 8.8 mm ID tube, spanning the area of the tube used as the test section for film thickness and wave measurements. Two strain-gauge based differential pressure sensors were connected in parallel so that the pressure gradient could be determined with low uncertainty across a wide range of flows. The pressure measurements were averaged over at least 15 s to account for fluctuations due to waves. Propagating both instrument and statistical uncertainties, the total uncertainty of the pressure difference measurement is of order 2%.

2.5. Film thickness measurement

Using a technique outlined by Shedd and Newell (1998), base film thickness measurements were made at the top, bottom, and side of the tube for each flow condition. This non-intrusive method uses the pattern of diffuse light reflected from the liquid surface to determine the liquid film thickness. Rodíguez and Shedd (2004) have shown, by comparisons with direct film measurements using planar fluorescence imaging, that this optical method accurately

determines the mean film thickness between large liquid waves. Uncertainties vary with the film thickness and surface roughness (waviness). Typical base film thickness uncertainties are around 2% for high gas flows and 5% for low gas flows, both within the fully annular regime.

2.6. Wave measurements

An optical method, similar to that reported by Hawkes et al. (2000), was used to study wave frequency, velocity and spacing. Two LED/phototransistor pairs were mounted on the outside of the tube, 0.115 m apart. Light from an LED passes through the transparent tube wall, through the air–water mixture and on to the phototransistor. When the surface of the liquid is not smooth, some of the light is refracted or reflected away from the phototransistor, causing a change in its output current. Using digital video imaging simultaneously with the LED/phototransistor measurement, it was confirmed that the phototransistor signal was very well correlated with liquid waves. Two wave sensors were used so that wave velocity and spacing could be obtained from the optical signals. A mean wave frequency, f_{wave}, was derived by analyzing the signal from each sensor individually using the fast Fourier transform (FFT) algorithm to generate a mean power spectral density for a large number of trials. By cross-correlating the signals, a wave velocity, v_{wave}, was derived. Between 100 and 250 trials were run for each annular test condition, each lasting between 1 and 2 s.

Occasionally, the cross-correlation of waveforms would pair incorrect waves in the two sensors, calculating an inaccurate velocity. The FFT algorithm would also occasionally calculate an incorrect frequency, usually a harmonic of the true frequency. This error was termed frequency doubling, as the first harmonic was most commonly found. In order to prevent a small number of data points from skewing the average, the largest and smallest 2–3% measurements were removed, generating a clipped mean. Within the annular regime, this clipped mean was very close to the median value.

3. Calculations

3.1. Experimental shear

For the fully annular data, it was found (Schubring and Shedd, submitted for publication) that wall shear is well correlated by

$$\tau_{w,SS} = 0.0217 \frac{KE_{sg}}{x} Re_G^{-0.15} = 0.0109 G U_{sg} Re_G^{-0.15} \tag{7}$$

This wall shear is required as an input for some of the wave correlations presented.

3.2. Correlations for wave velocity

An apparent direct relationship between wave behavior and shear (pressure drop) behavior was first observed by Swanson (1966), who found that the gas friction velocity, defined by Eq. (8) was equal to the wave velocity for his databank:

$$v_{fric,g} = \sqrt{\frac{\tau_w}{\rho_g}} \tag{8}$$

By using the correlation for wall shear developed for this data set, estimation of wave velocity as a function of gas superficial velocity, flow quality, and a total Reynolds number is indicated, producing the correlated friction velocity:

$$v_{fric,corr} = 0.104 \frac{U_{sg}}{\sqrt{x}} Re_G^{-0.075} \tag{9}$$

The dependence on total Reynolds number can be re-optimized to provide the correlation in Eq. (10):

$$v_{SS} = 0.42 \frac{U_{sg}}{\sqrt{x}} Re_G^{-0.25} \tag{10}$$

The Pearce correlation (Pearce, 1979) relates the wave velocity to surface film velocity, gas velocity, and a density ratio:

$$v_{wave,P} = \frac{u_{surf} + u_g \sqrt{\frac{\rho_g}{\rho_l}}}{1 + \sqrt{\frac{\rho_g}{\rho_l}}} \tag{11}$$

Neither the base film surface velocity nor the mean gas velocity are directly available from the present data. Therefore, direct application of Pearce's correlation is not possible. The graphical correlation of Shearer (1964) as replicated in Hall Taylor and Nedderman (1968) is not applied to the present databank as sufficiently high gas Reynolds numbers are not available in Shearer's work.

3.3. Correlations for wave frequency

Correlations based on dimensional analysis were created for the present databank. No single correlation attempted could successfully capture estimate wave frequency in all three tube diameters; possible reasons for this will be explored below. The correlations in Eqs. (12) and (13) were constructed; the former is for 8.8 and 15.1 mm data, while the latter is for the 26.3 mm data:

$$f_{SS} = 0.0050 \frac{U_{sg}}{D\sqrt{x}} \tag{12}$$

$$f_{SS} = 0.035 \frac{U_{sg}\sqrt{Fr_{mod}}}{D} \tag{13}$$

The modified Froude number is defined by Eq. (14):

$$Fr_{mod} = \frac{\rho_g U_{sg}}{\rho_l \sqrt{gD}} \tag{14}$$

4. Results and discussion

4.1. Wave velocity

Wave velocity for each tube diameter is plotted against U_{sg} in Fig. 2. Wave velocity increases with gas velocity and there is also a weak inverse proportionality with tube diameter. A liquid flow effect is also evident. Friction velocity and correlated friction velocity are shown in Fig. 3. In both plots, it is seen that some 26.3 mm data are not well correlated; these are also points for which reliable frequency data are not available. This may be indicative of smaller waves (see Section 4.4) leading to a weaker link between shear and wave behavior.

Due to the lack of direct measurements of mean gas velocity and film surface velocity, it is not possible to directly apply the Pearce model to the current data. As an estimate, a mean gas velocity based on a void fraction of 90% can be assumed, along with either the universal velocity profile or a laminar profile (based on average shear) within the base film. These two sets of assumptions each produce reasonable correlation to within 25% MAE (defined by Eq. (15)). This suggests further research in annular flow might properly center on measurement of film velocity profiles:

$$\mathrm{MAE} = \frac{1}{n}\sum_{i=1}^{n}\left|\frac{x_{\mathrm{corr},i} - x_{\mathrm{exp},i}}{x_{\mathrm{exp},i}}\right| \times 100\% \qquad (15)$$

However, both the gas velocity and liquid velocity along the interface are related to shear; direct correlation to shear is more successful, as both the friction velocity and correlated friction velocity produce an MAE less than 10%.

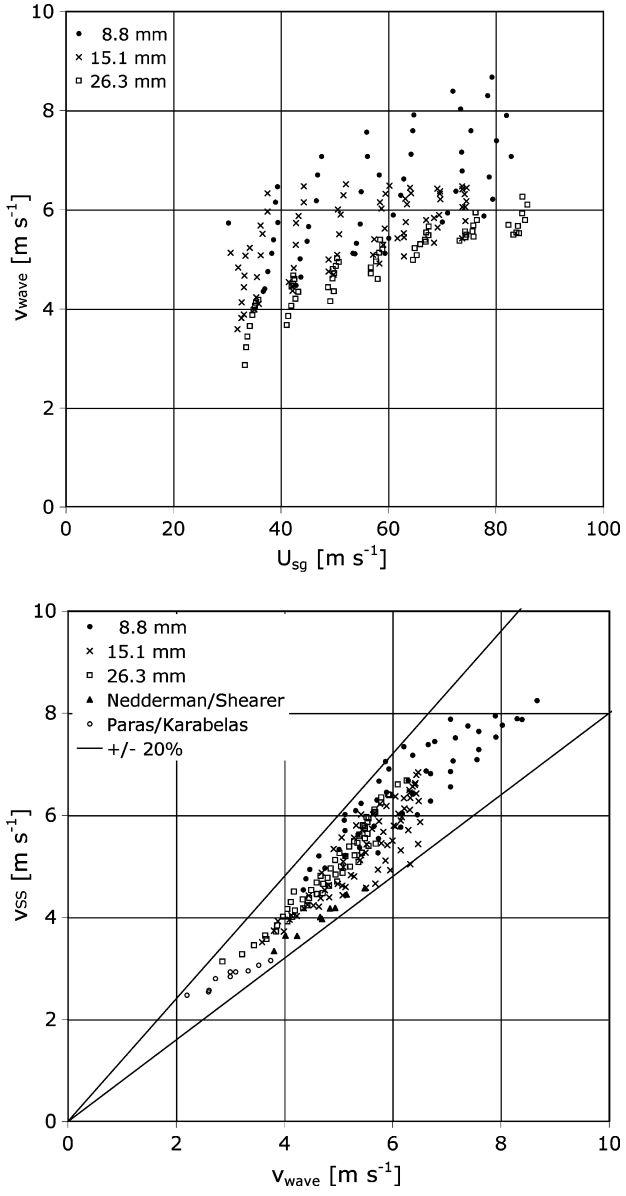

Fig. 2. Top: Superficial gas velocity vs. wave velocity. Bottom: Correlated wave velocity vs. measured wave velocity.

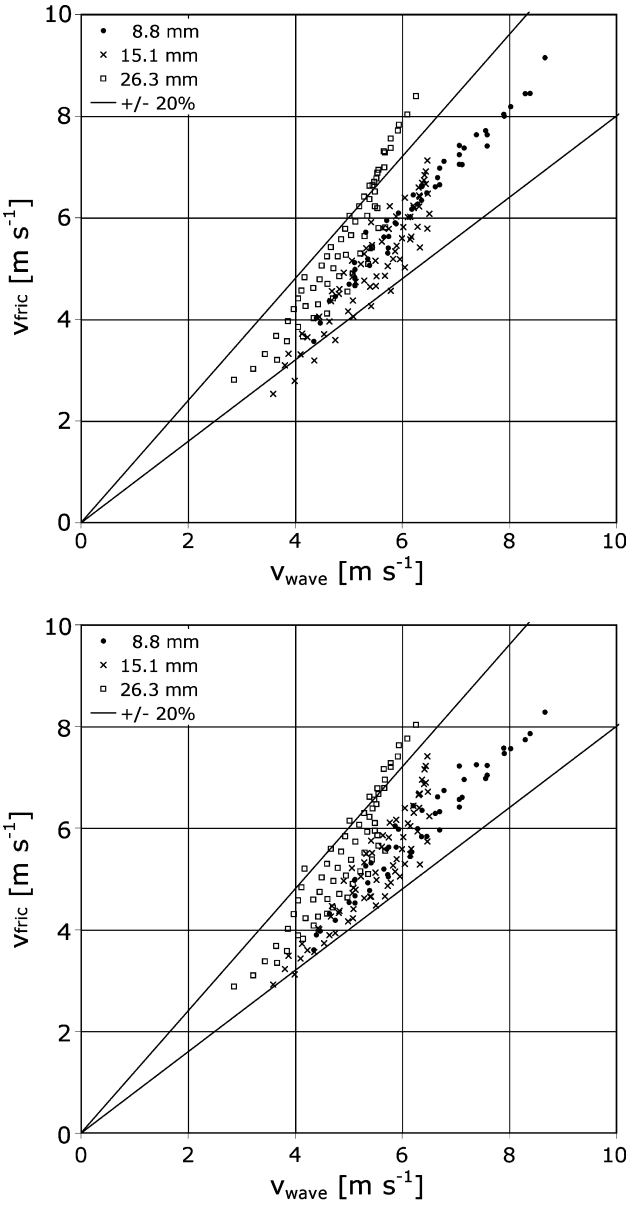

Fig. 3. Top: Friction velocity vs. wave velocity. Bottom: Correlated friction velocity vs. wave velocity.

The results of the present correlation (Eq. (10)) are shown in Fig. 2; the MAE of this relation is approximately 6%. It is a re-optimized version of the correlated friction velocity, with the power on Reynolds number modified to be more negative. This increases the dependence on diameter as seen in experiment, and also slightly improves performance within each diameter. The paper of Nedderman and Shearer (1963) regarding work in a 31.7 mm vertical test section provides a small amount of data within the liquid and gas superficial velocity range of the present correlation, which under-predicts velocity in this configuration by 9–17% for the available data. The velocity data of Paras and Karabelas (1991) within the flow rate range of the present study are predicted to within 8%. Both of these data sets are included in Fig. 2.

The correlation indicates that wave velocity would tend to increase with increased liquid viscosity. No data were available to investigate the viscosity effect; additional fluid pairs would need to be tested to confirm the Reynolds number dependence or to select another dimensionless group.

4.2. Wave frequency

Wave frequency is plotted against gas superficial velocity in Fig. 4. Shearer (1964) recommends expressing wave frequency as a form of Strouhal number (Eq. (16)) against a modified liquid Reynolds number (Eq. (17)):

$$Sr = \frac{f_{\text{wave}} D}{U_{\text{sg}}} \tag{16}$$

$$Re_{\text{L,Shearer}} = \frac{\dot{m}_{\text{l}}}{D\pi\mu_{\text{l}}} \tag{17}$$

If frequency were linearly proportional to gas superficial velocity for constant diameter and liquid Reynolds number (or superficial velocity), it would be expected that the plot of Strouhal number against modified Reynolds number would collapse to a line, or perhaps one line for each diameter. This is not seen for the present data.

Dimensional analysis suggests that wave frequency might be correlated by a function involving the ratio of a velocity and tube diameter. It is found that assigning gas superficial velocity as this characteristic velocity produces the best results. This is also suggested by the work of Azzopardi and Whalley (1980), who found that the volume of liquid in each wave decreases with increasing gas flow rate. Clearly, more waves are necessary to transport liquid as the wave volume decreases. A comparison of this characteristic frequency and measured wave frequencies is shown in Fig. 5. Estimating wave frequency as 1% of this characteristic frequency produces a correlation with an MAE of 17%.

Large ranges of Strouhal number at constant liquid Reynolds number as well as the spread in the frequency vs. characteristic frequency graph show that the correlation for wave frequency is not as simple as a velocity and diameter ratio. The dependence of wave frequency on gas superficial velocity indeed appears linear in the smaller tubes, but

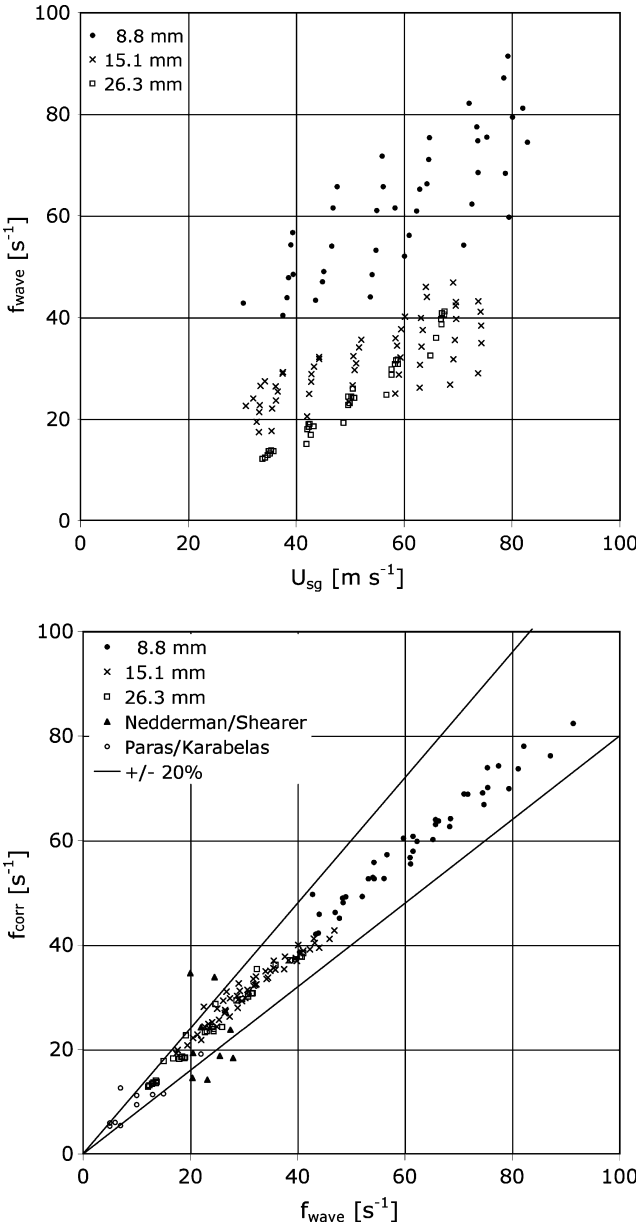

Fig. 4. Top: Superficial gas velocity vs. wave frequency. Bottom: Correlated frequency vs. measured frequency.

for the largest tube diameter, the frequency varies approximately as gas superficial velocity to the power 1.5. In the smaller tubes, there appears to be a quality effect not accounted for in the characteristic frequency; high quality flows show a strong over-prediction of wave frequency.

Due to the different behaviors, two separate correlations were developed. For the smaller tubes, Eq. (12) produces the best results, while Eq. (13) is better in the larger tube. The decrease in wave frequency with increasing tube diameter agrees with the observations of Martin (1983). The combined results of these correlations are shown in Fig. 4. A quality term was found to be adequate for correction of the characteristic frequency in the smaller tubes, but a factor of the square root of gas momentum (i.e., $\rho_{\text{g}} U_{\text{sg}} = Gx$) was found to be appropriate for the larger

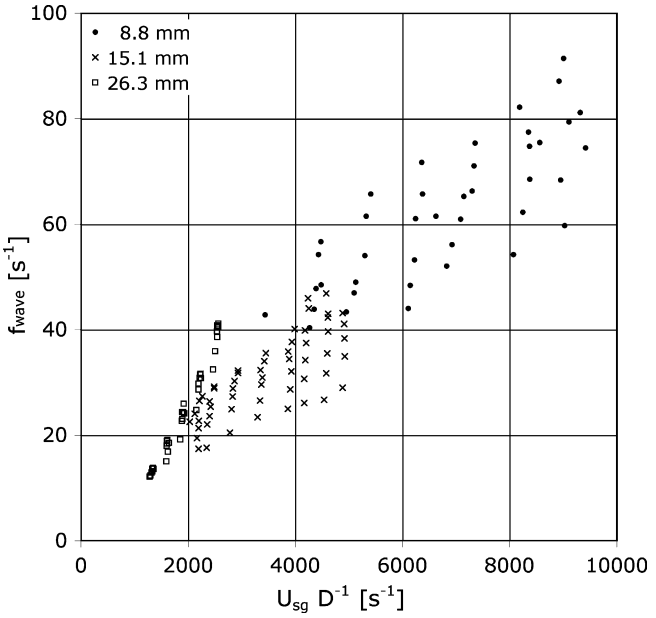

Fig. 5. Top: Frequency vs. characteristic frequency from dimensional analysis.

tube. The larger tube effect was phrased as a modified Froude number. The selection of this dimensionless parameter as opposed to, for example, a Reynolds number, is discussed in the section on lower KE_{sg} wave behavior.

Both correlations show an MAE below 6% and an RMS of below 7% for the portions of the current databank pertaining to their respective diameters. For the vertical data of Nedderman and Shearer (1963) and the horizontal data of Paras and Karabelas (1991) within the superficial velocity limits of the present study, the frequency correlation developed is accurate to within 25% MAE. These data are shown in Fig. 4.

Because data are not available to blend the correlations at intermediate diameters, care should be taken in selecting the appropriate correlation for interpolation between 16 and 25 mm. Further, the large-diameter correlation implies a dependence on density ratio that has not been fully explored. However, for vertical flow with similar tube diameter, Martin and Azzopardi (1985) note that wave frequency is seen to increase with the square root of gas density, as suggested by the present correlation. Additional research in other size tubes or with other fluid combinations would be required to refine these relations.

4.3. Wave spacing

Wave spacing was calculated as the ratio of wave velocity and wave frequency. The time-average wave velocity and wave frequency were used to calculate this quantity. Since correlations are available for both of these quantities, a separate correlation was not developed. Owing to the functional similarity of the frequency and velocity correlations for the smaller two tubes, the wave spacing at constant diameter varies over a relatively narrow range. For annular flow in the 8.8 mm tube, all wave spacings are between 0.093 and 0.118 m. The range in the 15.1 mm tube is somewhat larger, between 0.137 and 0.240 m.

By combining the frequency and velocity correlations and considering the diameter dependences in the dimensionless group, it is found that for the large-diameter correlation wave spacing is expected to increase linearly with diameter (for constant G, x, and properties). For the small-diameter correlation, it is found that spacing should increase with diameter to the power 0.75. A rough approximation for wave spacing (21% MAE) is 10 times tube diameter.

A second estimate of wave spacing can be made by taking the average of the wave spacing at each trial. It can be shown that this is equivalent to a wave-averaged spacing. For the 15.1 and 26.3 mm tubes, it was found that this estimate is larger than the time-averaged measurement (by an average of approximately 2%) for 89 of the 90 relevant flow conditions. In the 8.8 mm data, this trend was not replicated; the differences between the two estimates appeared to be distributed randomly about zero.

4.4. Inferences from wave detectability

The current experimental apparatus was unable to measure the frequency and velocity of waves accurately for some flow conditions. These included low liquid flow rates in all tubes and high gas flows rates in the largest tube. While this limited the amount of data that could be presented in the present paper, it also allows for inference to be made as to the nature of the waves. This apparatus is better suited to detecting large waves, as it is based on the scattering of light randomly by the chaotic disturbance waves, in contrast to the transmittal of light through base film.

It was seen in a number of flow conditions that velocity could be measured accurately while frequency could not. The reverse did not occur, indicating that accurate detection of wave frequency requires larger waves. This is likely due to light being scattered by both disturbance waves and ripples; isolating the disturbance waves is easier when they are much larger than the ripples. The wave velocity measurement, on the other hand, cross-correlates two signals of which the waves are the dominant feature.

Because the regions in which wave velocity could not be identified are bordered by regions in which velocity was detected but frequency was not, it would seem that the waves are smaller (or non-existent) in regions where they were not detected. Considering the excess liquid hypothesis, the high gas flow region may be indicative of high entrainment, while the low liquid flow region may indicate that the base film is sufficiently thick to transport the liquid. Rodríguez (2004) used PLIF imaging to visualize disturbance waves directly in a very similar flow loop, which provides information about their size. This work, also discussed by Rodíguez and Shedd (2004), indicated that the size of waves does not change with decreasing liquid flow rate. As such, the source of the increased

difficulty in wave data acquisition for low liquid flows is not entirely explained.

4.5. Lower KE_{sg} wave behavior

Disturbance waves are also present in the wavy-annular and wavy regimes. These flow regimes are characterized by greater asymmetry in film thickness distribution as compared to annular flow, as well as different shear behavior. Wavy-annular flow includes continuous wetting of the top of the tube; wavy flow does not. Further differences between annular and wavy-annular/annular flow are seen in wave behavior. Flows with KE_{sg} between 100 and 600 J m^{-3} were considered to be in the wavy-annular/wavy regimes. A total of 93 wave velocity measurements were available in these regimes, with 75 wave frequency measurements.

Both the friction velocity and the present wave velocity correlation generalize fairly well into these lower regimes. The friction velocity performs to within 16% (MAE), under-predicting most wavy/wavy-annular flows, particularly in the smallest tube and at the smallest gas flow rates. The present correlation tends to over-predict wave velocity, with the error increasing with decreasing gas flow. Considering all wavy/wavy-annular conditions, it predicts to within 13% (MAE), which improves to 10% if flow conditions without continuous top wetting are excluded. Plots of friction velocity and of the present correlation against measured wave velocity are shown in Fig. 6.

The difference in wave frequency behavior is more striking. Figs. 7–9 show the dependence of frequency on KE_{sg} for each series of constant liquid superficial velocity (flow

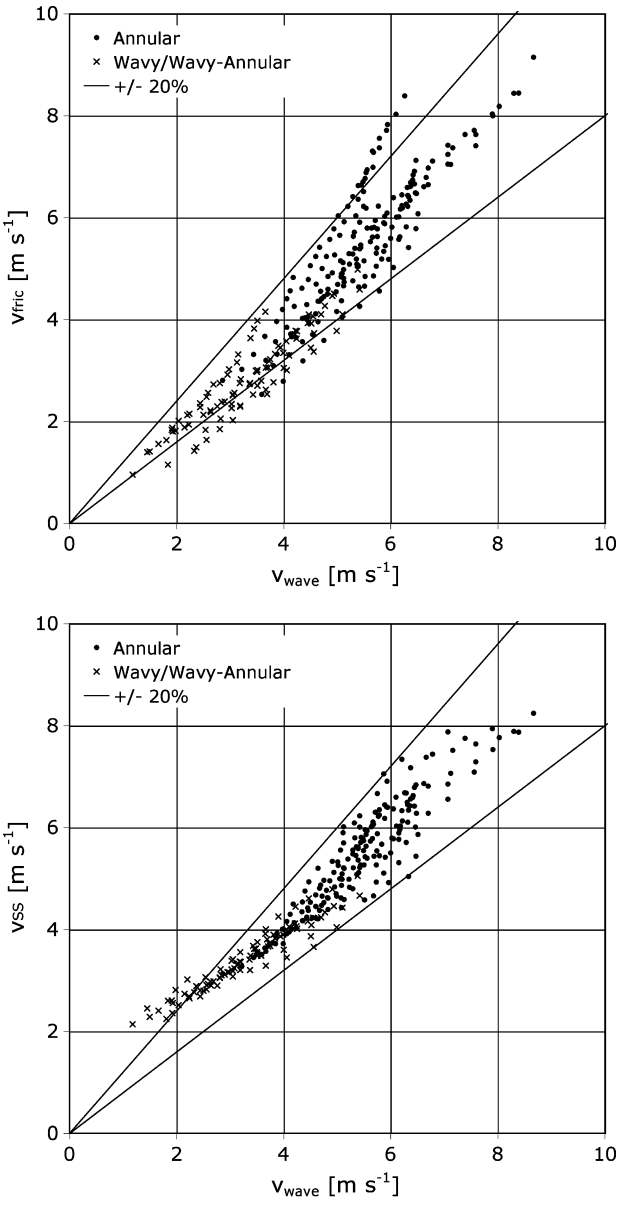

Fig. 6. (Including wavy-annular data) Top: Friction velocity vs. wave velocity. Bottom: Correlated wave velocity vs. wave velocity.

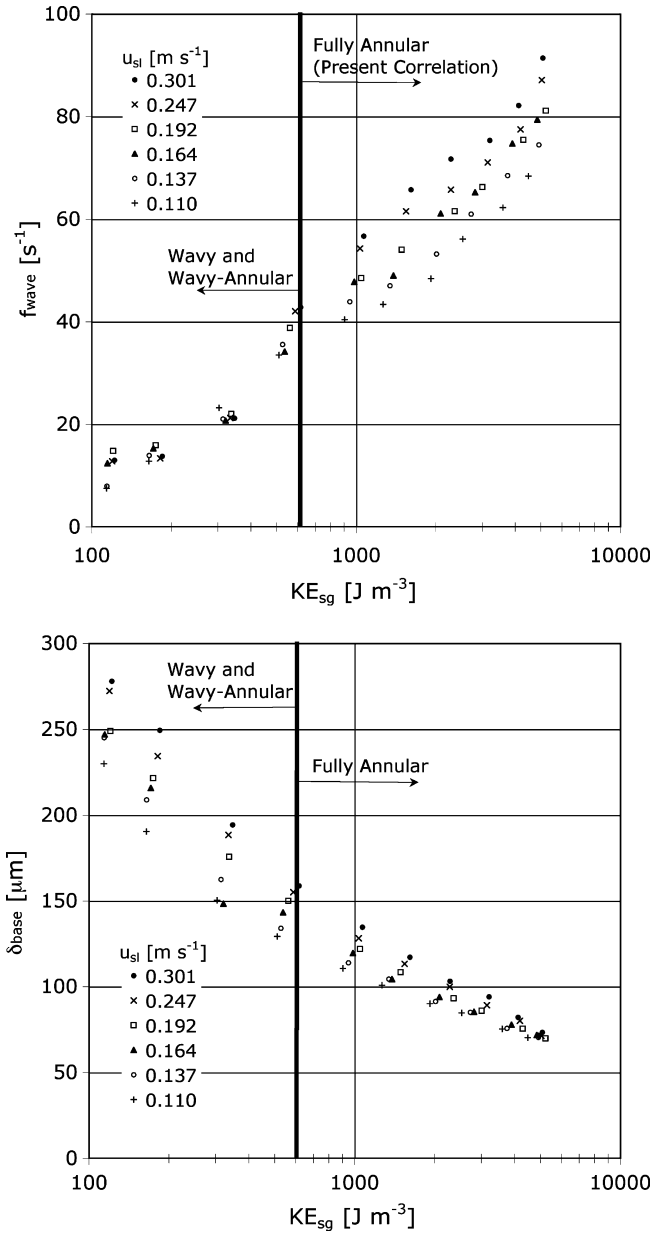

Fig. 7. 8.8 mm tube, series of constant liquid flow. Top: Wave frequencies against KE_{sg}. Bottom: Base film thickness against KE_{sg}.

rate) for the 8.8, 15.1, and 26.3 mm tubes, respectively. In contrast to the fully annular data, wavy and wavy-annular flows show a weak inverse relationship between wave frequency and liquid flow at constant gas flow. This relationship is sufficiently weak that when the increased occurrences of frequency doubling in the sensors are considered, the possibility that the wave frequency is a constant with respect to liquid flow cannot be excluded. This weak dependence of wave frequency on liquid flow may confirm the observation of Thwaites et al. (1976) that an asymptotic wave frequency with superficial velocity exists for flow conditions that are labeled wavy-annular in the present study.

The small-diameter correlation for wave frequency presented above does not generalize well into the wavy-annular and wavy regimes, showing an MAE of over 50%. However, the large-diameter correlation shows fair agreement, with an MAE of 21%. The large-diameter correlation is therefore recommended, except when the flow is fully annular ($KE_{sg} > 600$ J m^{-3}) and the tube diameter is less than 20 mm, in which case the smaller diameter correlation should be used. This produces an overall (all regimes, all diameters) MAE of 11% and is shown in Fig. 10. Examination of Figs. 7–9 in light of the performance of the two correlations indicates that one works when wave frequency is a weak function of liquid flow (e.g., 26 mm tube, wavy-annular) and the other when wave frequency is a stronger function of liquid (e.g., annular flow in 8.8 and 15.1 mm tubes).

Base film mean thickness is also shown plotted against in Figs. 7–9. In regions where wave frequency is a strong function of liquid flow, it is seen that base film thickness approaches a constant with KE_{sg}. In light of the excess liquid hypothesis, additional liquid is allowed to flow in

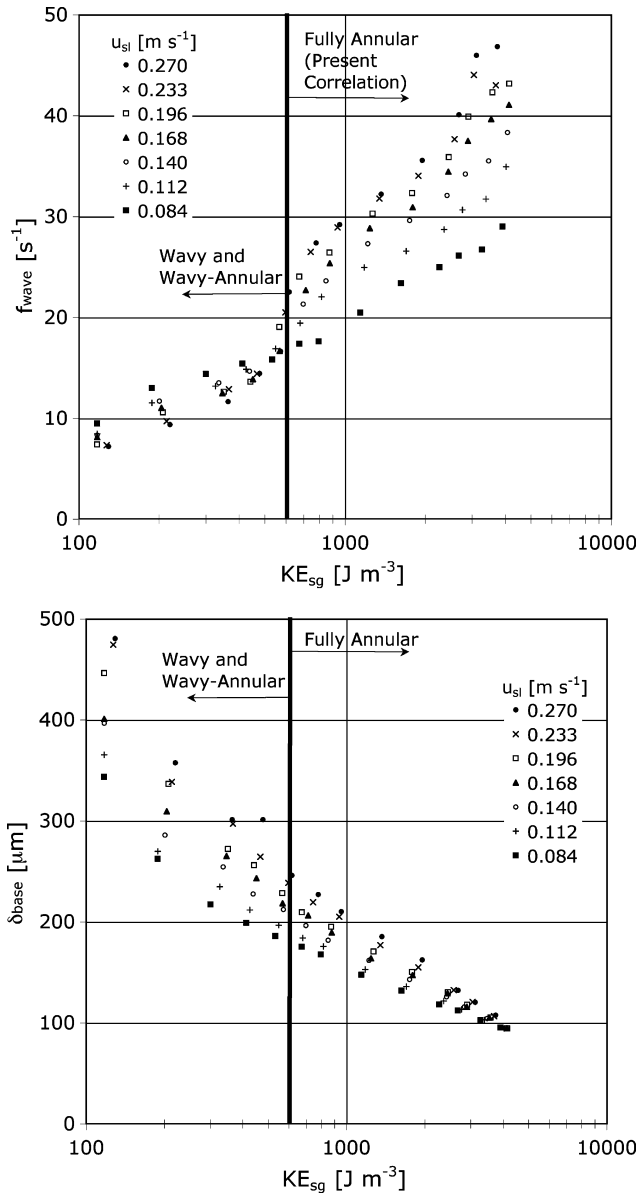

Fig. 8. 15.1 mm tube, series of constant liquid flow. Top: Wave frequencies against KE_{sg}. Bottom: Base film thickness against KE_{sg}.

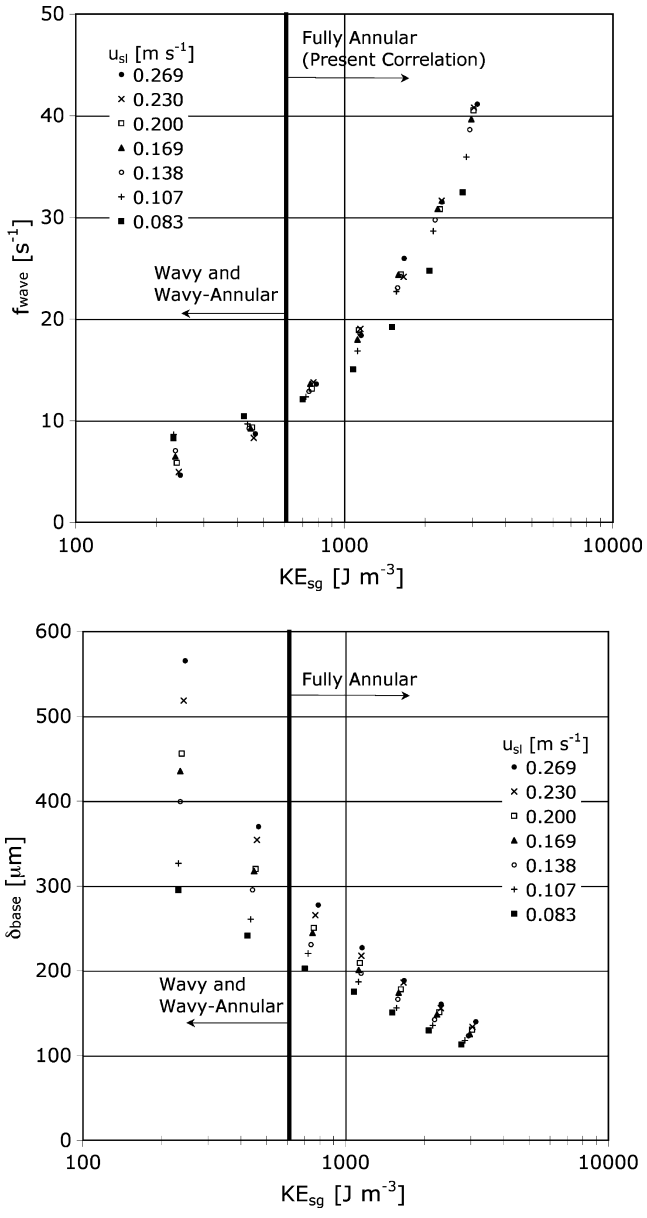

Fig. 9. 26.3 mm tube, series of constant liquid flow. Top: Wave frequencies against KE_{sg}. Bottom: Base film thickness against KE_{sg}.

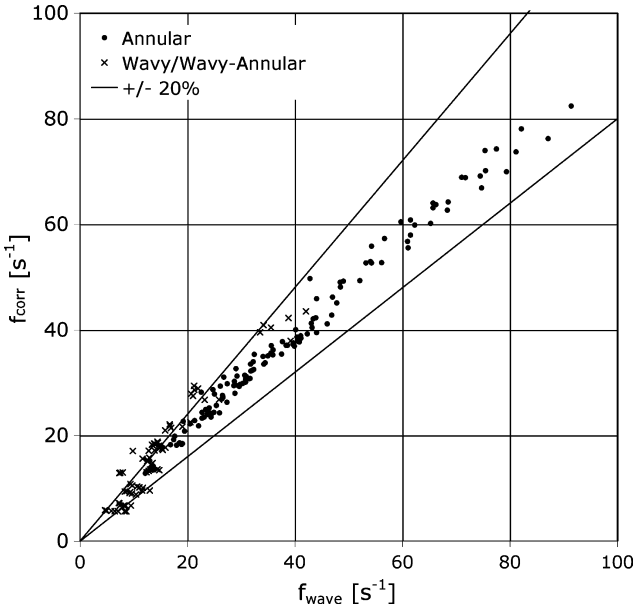

Fig. 10. (Including wavy-annular data) Correlated frequency vs. measured frequency.

the thickening base film for the wavy-annular regime, which does not require additional waves (i.e., the frequency need not increase). In contrast, for air–water fully annular flow, base film thickness becomes a function of KE_{sg} only. As such, additional liquid cannot flow in the film and must therefore generate the additional waves seen.

It is noteworthy that the same correlation performs well for wavy-annular flow in all tube diameters and for fully annular flow in large tubes. Because its regions of applicability are those for which gas momentum is smaller and/or diameter is large, a modified Froude number was selected as the dimensionless group to account for the non-linear gas superficial velocity effect. Additional fluid pairs would be required to explore the implied dependence on liquid density. Since wave spacing based on the larger diameter correlation is expected to vary linearly with diameter, this result can be generalized into the wavy-annular regime as well.

Frequency data were generally not available for very low liquid velocities using the present detection method, which did not allow for direct extension of the wave inception results of Nedderman and Shearer (1963) and others to the horizontal case. However, for the 26.3 mm case, it seems that these results are confirmed, in that wave frequency increases to an asymptote with increasing liquid flow at constant gas flow.

5. Summary

- Wave velocity is well correlated by the gas friction velocity within the fully annular regime, which may indicate a direct link between wave and wall shear behavior.
- An optimized correlation of similar structure to gas friction velocity (using a previous correlation for shear) can correlate the present databank of fully annular flow to within 6%.
- There are differences in the dependence of wave frequency on gas and liquid flow rates between tube diameters. Separate correlations can be developed for large and small tubes that correlate the current databank to within 6%.
- Wave velocity measurements in wavy-annular flow show similar trends to that in fully annular flow; both friction velocity and the present velocity correlation are accurate to within 20%.
- Wave frequency measurements in wavy-annular flow show fundamentally different behavior, particularly with respect to the trend with changing liquid flow.

Acknowledgements

The authors appreciate the financial support for the data acquisition portion of this project provided by the Petroleum Research Fund and the National Science Foundation under award number CTS-0134510. Any opinions, findings and conclusions or recommendations expressed in this material are those of the authors and do not necessarily reflect the views of the National Science Foundation.

References

Azzopardi, B.J., 1986. Disturbance wave frequencies, velocities and spacing in vertical annular two-phase flow. Nucl. Eng. Des. 92, 121–133.

Azzopardi, B.J., Whalley, P.B., 1980. Artificial waves in annular two-phase flow. In: Lahey, R.T., Rothe, P.H. (Eds.), . In: Proceedings of the Symposium on Basic Mechanisms in Two-Phase Flow and Heat Transfer, Chicago, vol. 129. ASME, New York, pp. 1–8.

Hall Taylor, N.S., Nedderman, R.M., 1968. The coalescence of disturbance waves in a annular two-phase flow. Chem. Eng. Sci. 23, 551–564.

Hall Taylor, N., Hewitt, G.F., Lacey, P.M.C., 1963. The motion and frequency of large disturbance waves in annular two-phase flow of air–water mixtures. Chem. Eng. Sci. 18, 537–552.

Hawkes, N.J., Lawrence, C.J., Hewitt, G.F., 2000. Studies of wispy-annular flow using transient pressure gradient and optical measurements. Int. J. Multiphase Flow 26, 1565–1582.

Jayanti, S., Hewitt, G.F., White, S.P., 1990. Time-dependent behavior of the liquid film in horizontal annular flow. Int. J. Multiphase Flow 16, 1097–1116.

Martin, C.J., 1983. Annular two phase flow. D.Phil thesis, University of Oxford.

Martin, C.J., Azzopardi, B.J., 1985. Waves in vertical annular flow. Physico-Chem. Hydrodyn. 6, 257–265.

Mori, K., Kaji, M., Kondo, Y., Sekoguchi, K., 1996. Wave venation in downward gas–liquid two-phase flow. Part I: Time-spatial behavior chart of interface and analysis of main wave-vein. Heat Transfer – Jpn. Res. 25, 499–510.

Mori, K., Kondo, Y., Kaji, M., Yagishita, T., 1999. Effects of liquid viscosity on characteristics of waves in gas–liquid two-phase flow (characteristics of huge waves and disturbance waves). JSME Int. J. Ser. B – Fluids Therm. Eng. 42, 658–666.

Nedderman, R.M., Shearer, C.J., 1963. The motion and frequency of large disturbance waves in annular two-phase flow of air–water mixtures. Chem. Eng. Sci. 18, 661–670.

Ottens, M., Klinkspoor, K., Hoefsloot, H.C.J., Hamersma, P.J., 1999. Wave characteristics during cocurrent gas–liquid pipe flow. Exp. Therm. Fluid Sci. 19, 140–150.

Paras, S.V., Karabelas, A.J., 1991. Properties of the liquid layer in horizontal annular flow. Int. J. Multiphase Flow 17, 439–454.

Pearce, D.L., 1979. Film waves in horizontal annular flow: space–time correlator experiments. CERL Note RD/L/N111/79.

Rodíguez, D.J., Shedd, T.A. 2004. Cross-sectional imaging of the liquid film in horizontal two-phase annular flow. In: 2004 ASME Heat Transfer/Fluids Engineering Summer Conference, Charlotte, NC, July 2004, Paper 56445.

Rodríguez, D.J., 2004. Characterization of bubble entrainment, interfacial roughness and the sliding bubble mechanism in horizontal annular flow. PhD thesis, University of Wisconsin-Madison, Madison, Wisconsin, USA.

Schadel, S., 1988. Atomization and deposition rates in vertical annular two-phase flow. PhD thesis, University of Illinois at Urbana-Champaign, Urbana, Illinois.

Schubring, D., Shedd, T.A., submitted for publication. Prediction of wall shear for horizontal annular air–water flow. Int. J. Multiphase Flow.

Shearer, C.J.,1964. PhD thesis, University of Cambridge, Cambridge, UK.

Shedd, T.A., Newell, T.A., 1998. Automated optical liquid film thickness measurement method. Rev. Sci. Instrum. 69, 4205–4213.

Swanson, R.W., 1966. Characteristics of the gas–liquid interface in two-phase annular flow. PhD thesis, University of Delaware, Delaware, June.

Thwaites, G.R., Kulov, N.N., Nedderman, R.M., 1976. Liquid film properties in two-phase annular flow. Chem. Eng. Sci. 31, 481–486.

Zanelli, S., Hanratty, T.J., 1971. Relationship of entrainment to wave structure on a liquid film. In: International Symposium on Two-Phase Systems, Haifa, Israel, August–September, vol. 2-1, pp. 2–22.